

*Journal of Neuroscience, in press*  
*September, 2013*

# **Cortical Surface Alignment in Multi-Subject Spatiotemporal Independent EEG Source Imaging**

**Arthur C. Tsai<sup>1\*</sup>, Tzyy-Ping Jung<sup>2,3</sup>, Vincent Chien<sup>1</sup>,**

**Alexander N. Savostyanov<sup>4</sup>, Scott Makeig<sup>2</sup>**

*<sup>1</sup>Institute of Statistical Science, Academia Sinica, Taiwan*

*<sup>2</sup>Swartz Center for Computational Neuroscience,  
University of California San Diego, La Jolla CA, USA*

*<sup>3</sup>Center for Advanced Neurological Engineering,  
University of California San Diego, La Jolla CA, USA*

*<sup>4</sup>State Research Institute of Physiology, SB RAMS, Novosibirsk, Russia*

**Key words:** ICA; EMSICA; cortically surface-based alignment, ERSP warping

\*Correspondence to: Arthur C. Tsai, Institute of Statistical Science, Academia Sinica, Taipei 11529, Taiwan. E-mail: [arthur@stat.sinica.edu.tw](mailto:arthur@stat.sinica.edu.tw)

## A B S T R A C T

---

Brain responses to stimulus presentations may vary widely across subjects in both time course and spatial origins. Multi-subject EEG source imaging studies that apply independent component analysis (ICA) to data concatenated across subjects have overlooked the fact that projections to the scalp sensors from functionally equivalent cortical sources vary from subject to subject. This study demonstrates an approach to spatiotemporal independent component decomposition and alignment that spatially co-registers the MR-derived cortical topographies of individual subjects to a well-defined, shared spherical topology (Fischl et al., 1999). Its efficacy for identifying functionally equivalent EEG sources in multi-subject analysis is demonstrated by analyzing EEG and behavioral data from a stop-signal paradigm using two source-imaging approaches, both based on individual subject independent source decompositions. The first, two-stage approach uses temporal infomax ICA to separate each subject's data into temporally independent components (ICs), then estimates the source density distribution of each IC process from its scalp map and clusters similar sources across subjects (Makeig et al., 2002). The second approach, Electromagnetic Spatiotemporal Independent Component Analysis (EMSICA), combines ICA decomposition and source current density estimation of the artifact-rejected data into a single spatiotemporal ICA decomposition for each subject (Tsai et al., 2006), concurrently identifying both the spatial source distribution of each cortical source and its event-related dynamics. Applied to the stop-signal task data, both approaches gave IC clusters that separately accounted for EEG processes expected in stop-signal tasks, including pre/postcentral *mu* rhythms, anterior-cingulate theta rhythm, and right-inferior frontal responses, the EMSICA clusters exhibiting more tightly correlated source areas and time-frequency features.

## Introduction

Independent Component Analysis (ICA) has been widely applied to blind separation of statistically independent processes in time-varying event-related response data including functional magnetic resonance imaging (fMRI) and electroencephalographic (EEG) signals, without making use of *a priori* knowledge of the spatial distributions or temporal properties of the sources processes summing to the observed responses (Hyvärinen, 1999; Makeig et al., 1996; Makeig et al., 1997; McKeown et al., 1998). To identify functional processes shared by a group of subjects, several group-level ICA approaches have been proposed for fMRI analysis (see Calhoun et al., 2009 for a review). To integrate EEG data across subjects, on the other hand, some studies have concatenated the subject data temporally by assuming the recorded electrode channel locations to be spatially equivalent across individual subjects (e.g., Kovacevic and McIntosh, 2007; Marco-Pallarés et al., 2005; Vakorin et al., 2010), while other studies have used spatial concatenation, implicitly assuming that each stimulus presentation and/or task-related response has occurred at the same latency across trials (e.g., Eichele et al., 2009; Eichele et al., 2008). The main feature of these approaches is to apply a single ICA decomposition to multi-subject data. However, it is well known that event-related EEG responses to stimulus presentations or time-locked to subject actions are in general not temporally consistent across trials, and their scalp topographies are not spatially consistent across subjects (for example, see Onton et al., 2005; Onton and Makeig, 2006). This is because the spatial projections of functionally equivalent cortical sources to the scalp electrodes can differ widely across subjects. As well, the peak latency, amplitude, and scalp distribution of all but the earliest brain responses to stimulus onsets can vary from one trial to the next within each subject, creating a data heterogeneity problem for multi-subject analysis.

An alternative approach to multi-subject ICA decomposition is to first perform single-subject ICA decompositions and then to cluster the resulting components into equivalence classes that share common spatiotemporal features (Langers, 2010; Makeig et al., 2002). However, a pair of either within- or between-subject derived independent components (ICs) may resemble and/or differ from each other in many respects – e.g., in their scalp maps, power spectra, event-related potential (ERP) time courses, and/or event

related spectral perturbation (ERSP) and inter-trial coherence (ITC) time/frequency images (Makeig, 1993; Makeig et al., 2004). The issue of how to find equivalent IC clusters or categories across subjects is thus theoretically non-trivial and may be viewed as an indeterminate problem in the ICA EEG analysis model itself, whose optimal solution depends on the nature of biological consistency across individuals as well as methodological efficiency.

ICs have been commonly clustered into homogeneous groups by comparing their scalp topographies, and several studies have proposed and assessed methods for clustering ICs according to their cortical locations estimated from the scalp topographies (De Lucia et al., 2010; Delorme et al., 2007; Knyazev et al., 2011; Makeig et al., 2002; Marco-Pallarés et al., 2005; Milne et al., 2009; Onton et al., 2005; Pockett et al., 2007; Ponomarev et al., 2010). The source imaging methods applied in these studies are mainly performed in a two-stage manner, e.g. as supported by the EEGLAB software environment (Delorme and Makeig, 2004). First, ICA decomposes the data from a cognitive task of interest into temporally and in many cases functionally distinct IC processes. Then, to assist in anatomic and functional interpretation of the component process a source localization/imaging method is used to estimate the cortical locations of the individual ICs from their scalp maps given by the individual columns of the ICA unmixing matrix. For example, each component may be modeled as one (or occasionally two) equivalent current dipoles (e.g., Makeig et al., 2002; Milne et al., 2009; Onton et al., 2005; Pockett et al., 2007; Ponomarev et al., 2010; Zhukov et al., 2000), or as a current-source density distribution (e.g., Congedo et al., 2010; De Lucia et al., 2010; Delorme et al., 2007; Marco-Pallarés et al., 2005; Ponomarev et al., 2010).

However, identifying equivalent ICs by directly clustering either their scalp maps or equivalent dipole locations computed from the identified IC scalp maps may be prone to error; a group of ICs may have similar scalp maps but functionally different source locations, and functionally equivalent cortical sources may have quite different brain and scalp distributions. Figure 1 illustrates this problem. Fig. 1 shows a simulated EEG source (top row) consisting of mixtures of two Gaussian-tapered cortical patches (occupying approximately  $163.7 \text{ mm}^2$  in the superior parietal gyrus) based on a group-averaged inflated model in the left hemisphere cortex, and its projections onto the

spherical topographies of five subjects using the FreeSurfer cortical area parcellation applied to five subjects' MR head images (MGH, Harvard Medical School, available from <http://surfer.nmr.mgh.harvard.edu>; Dale et al., 1999; Desikan et al., 2006; Destrieux et al., 2010; Fischl et al., 1999). FreeSurfer reconstruction has been widely used in EEG/MEG source imaging analysis over the last few years, e.g., in the MNE software (Hämäläinen, 2009) that computes cortically-constrained L2 minimum-norm current estimates from MEG/EEG signals, allowing group analyses to be computed in the same space.

Here, as shown in Fig 1, by identifying and warping the subject cortical models to a common template (topmost), the prominent cortical sulci of the inflated cortical models of our five subjects (row 2) after co-registration of their major sulci. Below this are shown the locations on the five original fully-inflated (row 3) and native (not-inflated, row 4) cortical models for each subject, and below these, the scalp projection (scalp map) for each of these functionally equivalent sources, as computed using boundary element method (BEM) forward electrical head models constructed from an MR head image for each subject (Akalin Acar and Makeig, 2010). Because details of cortical topology and folding differ across the subjects, both the spatial locations and orientations of equivalent cortical areas and their scalp projections vary widely. The lowest two rows show the equivalent current dipole (Scherg and Von Cramon, 1985; Scherg and Voncramon, 1986) for each simulated component scalp map in a standard MNI template brain (Maintz and Viergever, 1998), computed using *dipfit()* (Oostenveld and Oostendorp, 2002) in EEGLAB, and sLORETA-computed source current density distributions in the individual subject cortical surface models (Pascual-Marqui, 2002). The topological (and presumed functional) equivalence of the five simulated sources is not apparent either from the component scalp maps, equivalent dipole source locations, or distributed sLORETA source current density estimates.

This inter-subject spatiotemporal heterogeneity of functionally equivalent cortical sources and their scalp projections raises an important question about how best to perform multi-subject source-level comparison in EEG studies. However, Fig. 1 also suggests a possible solution. Here, unlike the now conventional two-stage approach that localizes the cortical source of each IC from its scalp map, we use spatiotemporal

EMSICA decomposition to decompose directly the continuous or concatenated trials EEG data into spatiotemporal components whose active source areas are identified by a distribution of cortical voxels on a MR-image derived model of the individual cortical surface. The so-identified active IC source areas are then spatially registered across subjects within a common spherical inflated-cortex model to which the individual cortical surface models have been warped and co-registered. Their event-related dynamics, in the form of ERSP and ITC images, are then co-registered on a common latency/frequency grid.

The Methods section below gives an overview of single-subject ICA approaches to EEG source localization and imaging, followed by a detailed elaboration of the spatiotemporal alignment scheme and its use for multi-subject comparison. The proposed cortical alignment scheme is applied to ICs identified in an experimental data set using two decomposition approaches, one a conventional two-stage approach using IC scalp maps contained in the temporal ICA unmixing matrix to estimate IC source densities (Makeig et al., 2002). The other is the Electromagnetic Spatiotemporal Independent Component Analysis (EMSICA) method that combined temporal ICA decomposition and source density estimation into a single spatiotemporal model estimation process (Tsai et al., 2006).

The experimental data were collected from eleven participants in a self performance-monitoring and -inhibition stop-signal paradigm (SSP) (Logan et al., 1984; Savostyanov et al., 2009). The results included spatiotemporal ICA component processes in visual, motor, frontal and anterior cingulate cortical areas. The significance of the cortical activation topographies and directions for future work on the multi-subject EEG source imaging are highlighted.

*Figure 1. Differences in cortical locations and scalp maps for functionally equivalent simulated ICs.*

## Methods

The step-by-step procedure of our proposed multi-subject EEG source imaging analysis approach includes: (a) realistic single-subject forward electrical head modeling, (b) single-subject EEG data preprocessing and spatiotemporal independent source decomposition (either using ICA followed by source localization or projection of the data onto the cortical surface followed by EMSICA), followed by, (c) multi-subject cortical surface alignment, (d) event-related spectral perturbation (ERSP) and/or other measure computation using, if relevant, (e) trial-to-trial latency alignment, and finally, (f) IC source clustering.

### *Experiment design*

Eleven healthy right-handed males (ages  $26 \pm 3$  years) participated in a stop-signal (SSP) experiment to investigate brain active source areas and associate event-related power changes involved in rapid motor response initiation and inhibition. Participants were presented with a picture (a deer or a tank) at roughly 4-s intervals and were asked to respond to each picture by pressing one of two buttons using their right or left thumb, respectively, thereby choosing a weapon (a rifle or an anti-tank rocket launcher) to shoot at the target (Savostyanov et al., 2009). The ‘deer’ and ‘tank’ stimuli were presented in random order with equal probability at inter-stimulus intervals randomly varying between 3.5 s and 5.5 s. In 30 of the 130 trials, target presentation was followed by a stop-signal cue indicating that the participant should not press either button; that is, cueing them to refrain from their prepared motor response. The interval between onset of the picture and stop-signal randomly varied between 250 ms and 538 ms. Trials containing response errors (mean 4.2; min 1, max 14) were removed from the analysis. Here we considered two task conditions – “press” (when the participant pressed the button after target stimulus presentation), and “stop” (when he successfully suppressed his response following stop-signal presentation).

### *Data collection*

EEG data were recorded using a Neuroscan Synamps2 amplifier; 3-D positions of the EEG electrodes were digitized using a Polhemus FASTRAK 3-D digitizer. The high-density physiological data were recorded using a 131-channel Quik-cap, Neuroscan, El Paso, TX, with 128 scalp EEG plus peri-ocular VEOG and HEOG, and chest EKG reference signals. The data were bandpass filtered (0.1–100 Hz; 60-Hz notch filter enabled) and digitized at 1000 Hz with 32-bit resolution. The ground electrode was placed midway between Fz and Cz. The online reference was acquired from an electrode mounted between Cz and CPz. The subjects were also given T1-weighted (T1-TFE 3-D sequence) structural MR head scans in a Philips 3-Tesla scanner.

### *Electrical head modeling*

Realistic head modeling relies on accurate segmentation of anatomical MR images into tissue types with differing conductivities. Construction of realistic head models for single subjects allows for between-subject variability in conductor tissue volumes and geometry to be taken into account in source imaging. For this purpose here we used NFT (Akalin Acar and Makeig, 2010) and FreeSurfer (Dale et al., 1999). The next few sections detail these and other steps in the procedure.

For each subject, a lead field matrix (see Eq. (5) below) was calculated from a high-quality realistic boundary element method (BEM) head model. Forward model computation for the complex, electrically heterogeneous human head relies on the ability of segmentation and tessellation algorithms to identify compartment boundaries between tissue types including brain tissue vs. CSF, CSF vs. skull, skull vs. scalp, and scalp vs. air. It also requires estimates of the relative conductivities of these model compartments. The pial surface model as well as boundaries between three other tissue types (CSF, skull, and scalp) were reconstructed using the BET2 software package (Jenkinson et al., 2005; Smith, 2002) using approximately 2,562 vertices randomly distributed in each layer to produce the high-quality linear surface BEM meshes used in the subsequent lead field computation. We assumed homogeneous isotropic conductivities of 0.33, 1, 0.0042, and 0.33 ( $\Omega m$ )<sup>-1</sup> for brain, CSF, skull, and scalp, respectively (Mosher et al., 1993). The

white matter layer was semi-automatically reconstructed using the FreeSurfer software package (Dale et al., 1999; Fischl et al., 1999) from a high-resolution T1-weighted structural MR image. The space of possible source distributions comprised 40,960 equivalent current dipoles centered at approximately decimated points on the white matter surface, each representing approximately  $4.8 \text{ mm}^2$  of the cortical surface, and oriented normal to the local cortical surface.

### *Preprocessing EEG data for source imaging*

For EEG source imaging, it is desirable to preprocess time varying signals by removing artifacts resulting from body movements, muscle and heart activity, and eye movements. Using ICA (or to a limited extent, PCA), EEG data can be separated into two parts, brain-related source signals and non-brain artifact signals. This separation may be accomplished by comparing the time courses of the component signals with reference signals collected from around the eyes and/or over the heart, by visual inspection of the component time courses, their power spectra, and/or scalp maps, and/or their ERP, ERSP or other event-related response measures (Jung et al., 2001). ICA has been found to be more effective than PCA for this purpose because of its ability to focus component filters on individual sources with maximally distinctive activity time courses (McKeown et al., 1998). Specifically, using ICA an unmixing matrix  $W$  decomposes the original data  $x^{(t)}$  collected from  $M$  sensors at time  $t$  into maximally temporally independent signals (ICs),

$$u^{(t)} = Wx^{(t)} \quad (1)$$

By simple matrix algebra, Equation (1) can be expressed as

$$x^{(t)} = Au^{(t)} \quad (2)$$

where  $A = W^{-1}$  denoting the mixing matrix whose columns can be partitioned into  $A = [A_A, A_B]$  with  $A_A$  of order  $M$ -by- $(M-K)$  denoting a collection of columns in  $A$  corresponding to noise or artifacts, and  $A_B$  of order  $M$ -by- $K$  corresponding to brain signals. The artifact-free EEG recordings at time  $t$  can be computed as follows:

$$x_c^{(t)} = A_B u_B^{(t)} \quad (3)$$

where  $u_B^{(t)}$  is the sum of the potentials back-projected from the non-artifact ICs to the

electrodes by the brain sources.

Here, preprocessing of each subject's data was performed in EEGLAB (Delorme and Makeig, 2004). After band-pass filtering (1-50 Hz, using an FIR filter, *eegfilt()*, in EEGLAB), the extended infomax ICA algorithm (Lee et al., 1999) was applied to all 131 scalp-channel signals across 130 concatenated trials, each trial including data from 1.0 s before to 2.5 s after picture onsets. Separation of brain signals from non-brain artifacts (e.g., eye movements and electrocardiographic activity) was performed using an automated approach that compared the IC time courses to the time courses of the three reference channel signals. A correlation value between an IC time course and that of a reference channel was computed to determine whether the IC accounted more for the non-brain artifact than for brain source signals. In this case the IC was excluded from further analysis. ICs accounting for myogenic artifacts were identified by visual inspection of their scalp maps and time courses, and were then removed to avoid their presence in the data substantially distorting estimates of active cortical source areas. In this step, only clearly identifiable non-brain artifacts were removed. The rest of the data were then back-projected to the scalp channels for further source separation and localization by EMSICA.

### *Spatiotemporal independent source imaging*

To estimate the source locations and/or distributions of the effective cortical source generation areas from  $x_c^{(t)}$ , parametric (e.g., dipole-fitting, Moshier et al., 1992; Scherg and Von Cramon, 1985; Scherg and Voncramon, 1986) and distributed source imaging methods (e.g., weighted minimum-norm, WMN, Hämäläinen and Ilmoniemi, 1994; Ioannides et al., 1990; Jeffs et al., 1987; Wang et al., 1992; standardized low-resolution electromagnetic tomography, sLORETA, Pascual-Marqui, 2002; or low-resolution electromagnetic tomography, LORETA, Pascual-Marqui et al., 1999) are the two principal approaches used to estimate solutions to the EEG inverse problem, which is typically posed as a problem of estimating a course source distribution for a map representing a peak in an evoked response (Baillet et al., 2001). The two-stage ICA-based EEG source imaging approach (temporal ICA decomposition followed by either

parametric or distributed source imaging methods) can be used to estimate the locations of multiple ongoing source EEG processes that contribute to ERPs, ERSs, and/or other measures.

The value of ICA for source localization lies in the fact that many IC scalp maps strongly resemble the projection of coherent local field activity within a small single (or sometimes dual) cortical area (Delorme et al., 2012), whereas peaks in average event-related potential (ERP) waveforms with post-event latencies of more than a few tens of milliseconds typically sum contributions from a number of cortical areas. Thus, ICA provides a basis set of ‘simple’ brain sources (in addition to separate non-brain and noise processes). Using ‘complete’ ICA decomposition (yielding the same number of source ICs as channels in the data) assumes that the cortical processes contributing to event-related dynamics of interest have sufficiently distinctive time courses to attract an IC filter. As the number of recording channels is decreased, complete ICA decompositions must inevitably begin to pass activity from more than one such cortical process. In practice, however, ICs making largest contributions to ERPs of interest are typically those with highly ‘dipolar’ scalp maps compatible with the projection of activity within a small source patch.

**Parametric source localization** typically assumes that the sources can be represented by one or at most a few equivalent current dipoles, each with an unknown location  $\gamma_i$  and orientation,  $\theta_i$ . For the simultaneous activation of multiple dipoles, it is possible to connect sources to the cleaned data specified in (3)

$$x_c^{(t)} = A_B u_B^{(t)} = G(\{\gamma_i, \theta_i\}) s^{(t)} \quad (4)$$

where  $G(\{\gamma_i, \theta_i\}) \in R^{M \times K}$  is the so-called gain matrix and  $s^{(t)} \in R^K$  denotes a collection of sources  $s_k^{(t)}$ ,  $k = 1, \dots, K$ . Each column of  $G(\{\gamma_i, \theta_i\})$  relates the activity of one or more equivalent dipoles to the array of sensor measurements and is called the forward field, gain vector, or scalp topography, of the single or distributed current dipole source sampled by the  $M$  discrete locations of the sensors (Baillet et al., 2001).

**Distributed source imaging** involves a solution to the following linear system

$$x_c^{(t)} = A_B u_B^{(t)} = LBs^{(t)} \quad (5)$$

where  $L \in R^{M \times J}$  is the so-called lead field matrix relating  $J$  dipolar source activity to the  $M$  recorded scalp potentials and  $B \in R^{J \times K}$  whose columns,  $b_k$ , for  $k = 1, \dots, K$ , contain relative weights describing the topography of locally synchronous (or partially synchronous) field activity on the cortical surface that contribute the component signals to the scalp recordings.

To find and display the vertices in the distributed source map that belong to this topography, the map values are normalized to  $z$  scores. By dividing the dipole strength estimate for each grid element by the standard error of the estimate, a normalized estimate of dipole strength can be obtained that is  $t$  distributed under the null hypothesis of no dipole activity (see Beckmann and Smith, 2004 for details). For comparison purposes, this procedure was followed for both the LORETA and EMSICA inverse solutions. Activation regions whose absolute  $z$  scores were larger than some threshold ( $|z| > 2.0$  in this empirical study here, the same as in Tsai et al., 2006) were considered to be active voxels that were color-coded in the component cortical maps.

### *The two-stage temporal ICA-based approach versus EMSICA*

In essence, the two-stage ICA approach assumes that the sources  $s_k^{(t)}$  in (4) or (5) are temporally independent, such that  $s_k^{(t)} = u_{k \in B}^{(t)}$  and solves  $A_B = G(\{\gamma_i, \theta_i\})$  or  $A_B = LB$  by performing inverse modeling of individual columns in  $A_B$  corresponding to the scalp maps. The spatiotemporal framework of EMSICA, by contrast, uses the cleaned EEG signals,  $x_c^{(t)}$ , in (5) as training data to estimate a matrix  $B$  that permits a trade-off between the temporal independence of their corresponding source time courses,  $s_k^{(t)}$ , and the spatial independence of underlying cortical source topographies,  $b_k$ , for  $k = 1, \dots, K$  (Tsai et al., 2006). The unknown source activation topography,  $B$ , can be estimated by maximizing the following posterior likelihood assuming spatial as well as temporal independence over the continuous data or concatenated set of data trials (at times,  $t = 1, \dots, T$ ),

$$p(B|x^{(t)}, L) \propto p(B) \int ds^{(t)} p(x^{(t)}|L, B, s^{(t)})p(s^{(t)}) \quad (6)$$

For EMSICA decomposition, the elements in the  $k$ th column of  $B$  are considered to be a realization of the random variable  $b_k$ . EMSICA assumes that those variables are spatially (maximally) independently distributed with distribution  $p_k(b_k)$  such that

$$p(B) = \prod_k p_k(b_k) \quad (7)$$

The prior  $p_k(b_k)$  is a probabilistic model that summarizes the spatial properties of an individual source. Here, super-Gaussian spatial as well as temporal probability density assumptions were used, i.e.  $p_k(b_k) \propto \exp\{-\beta f(b_k)\} \text{sech}^2(b_k)$  and  $p_k(s_k^{(t)}) \propto \exp\{-(s_k^{(t)})^2\} \text{sech}^2(s_k^{(t)})$ , where  $f(b_k) = b_k C^{-1} b_k^T$ ,  $C^{-1}$  is the spatial covariance of  $J$  tessellation elements and  $\text{sech}$  is the hyperbolic secant. In addition, for comparison purposes,  $f(b_k)$  in the spatial prior was chosen to be the same as that of the LORETA inverse solution, which also uses a Laplacian operator to emphasize the contribution of distributed, locally synchronous (or partially synchronous) current source activations.

Compared to EMSICA, the two-stage ICA approach, which involves performing source localization one IC at a time (column by column of the mixing matrix  $A_B$ ), dramatically reduces training data information for source analysis from  $x_c^{(t)}$ , for  $t = 1, \dots, T$ , to  $A_B$ , where the number of data points are  $M$ -by- $T$  and  $M$ -by- $K$ , respectively, while  $T \gg K$ . Such reduction makes the indeterminate nature of the inverse problem more difficult to resolve because the number of parameters to be estimated in the weight matrix,  $B$  of order  $J$ -by- $K$ , is much larger than the number of training data points in  $A_B$  of order  $M$ -by- $K$ .

However, EMSICA introduces into the training data errors produced by errors in the forward head model, whereas ICA is trained on the scalp data themselves, avoiding errors introduced by the head model which then come into play during the source localization of the IC scalp maps. The methods comparison performed here attempts to evaluate, for this data set, the quality of the results of the two approaches.

Meanwhile, as demonstrated in Fig. 1, even when the locations of the active source areas from different subjects have the same intrinsic topological (and likely, functional) positions in cortex (Fischl et al., 1999), between-subject differences in brain geometry may lead them to have significantly different scalp maps. When such scalp maps are used

for source analysis based on a standard brain template (e.g., an MNI brain template; Maintz and Viergever, 1998), either by dipole-fitting or distributed source imaging, ambiguous source-localization results may follow, as illustrated in Fig. 1.

In sum, EMSICA potentially offers a new and promising approach to source imaging, working directly on single-trial EEG data made artifact-free by an initial ICA decomposition, that estimates maximally spatiotemporally independent functional processes and, simultaneously, their corresponding current source densities. The spatiotemporal framework of EMSICA makes it possible to map single-trial EEG recordings onto a cortical surface model for each subject.

#### *Co-registration of IC active source areas across subjects*

Each cortical hemisphere can be represented as a topological 2-D sheet or sphere with more than two-thirds of its area buried in steep sulcal valleys. Cortical connectivity and function is effectively modular. Between-subject differences in 3-D cortical geometry make between-subject co-registration of cortical areas difficult and the problem of identifying equivalent IC activations from different subjects on the co-registered topological sheet or sphere by no means trivial. Most EEG source analysis approaches to the problem of finding clusters of equivalent IC across subjects have attempted to match one or more observed active source distributions or their equivalent dipole models in a 3-D standard head model using Talairach registration (Talairach, 1967; Talairach and Tournoux, 1988). These clustering approaches typically attempt to minimize the cortical distance between ICs assigned to a single cluster. However, directly measuring the distance in 3-D space between two cortical points may underestimate their actual distance on the highly folded cortical surface.

***Figure 2. An IC accounting for precentral mu rhythm (in the rPREC $\mu$  cluster), with and without group cortical alignment, shows differences in active cortical area across participants.***

To increase statistical power of clustering either temporally or spatiotemporally independent components, we here demonstrate use of a natural cortical surface-based coordinate system (Fischl et al., 1999). Figure 2 illustrates the cortical alignment procedure. The inflated image in Fig. 2a is the reconstructed right cortical hemisphere surface for Subject 2 in Fig. 1, with the active area of one IC source as estimated by EMSICA marked in red. This hemispheric model derived from an MR head image using cortical inflation tools in FreeSurfer (Dale et al., 1999) and then transformed into a sphere as shown in Fig. 2b using a method that minimizes metric distortion (Fischl et al., 1999). The warped light and dark gray areas, indicating major gyral and sulcal cortical landmarks, respectively, then form a natural coordinate system for co-registering individual surfaces and for constructing the average surface. Blue lines in Fig. 2c show an overlay of the group-mean sulcal/gyral boundaries (found by warping the individual cortical models to a common pattern onto the single-subject cortical model as implemented in the FreeSurfer utility function *make\_average\_subject()*). In Fig. 2d the subject's inflated cortex model and active IC source area have been warped (using a combination of FreeSurfer's *mri\_surf2surf()* using the 'nearest-neighbor, forward and reverse' argument, plus custom MATLAB code) so as to align the subject cortical surface to the group-mean surface by co-registering major sulcal and gyral landmarks.

#### *Event-related measure latency alignment*

Event-related changes in EEG source dynamics rapidly spread from an initial (e.g., specific sensory processing) focus to perturb the statistics of field dynamics in widely distributed cortical and sub-cortical areas (Klopp et al., 2000). Mean event-related signal measures capture different aspects of the perturbations in EEG source signal statistics time-locked to some set of experimental events (e.g., presentations of similar stimuli or subject responses occurring under similar task conditions). To overcome the variability in time delays in initiation of some underlying process in single trials, dynamic time warping has been used over the past few decades (Huang and Jansen, 1985; Picton et al., 1988; Roberts et al., 1987; Wang et al., 2001). The approach involves linear or nonlinear expansion and/or compression of the time axis of selected EEG trial segment waveforms. Note that if this is applied to the time domain data, it may change their power spectral

distribution.

The event-related spectral perturbation (ERSP; Makeig, 1993), giving a time/frequency image of mean event-related changes in the EEG power spectrum, can characterize significant event-related power changes (measured as log power differences) from the pre-stimulus mean (log) baseline spectrum. Here, instead of expansion or compression of the time axis of the EEG waveforms, a linear time-warping procedure (Gwin et al., 2011; Makeig et al., 2007) was applied to the single-trial ERSPs. That is, the common-baseline normalized event-locked single-trial spectrograms for each component source were firstly computed. The single-trial spectrograms were then linearly time-warped in such a way that sequences of events of interest (here, stimulus onset and ensuing stop signal presentation or participant button press) occurring in each trial were latency-aligned to allow across-trial averaging.

Applying such latency alignment to the single-trial ERSPs (normalized log spectrograms) can avoid smearing and possible cancellation of event-related power increases and decreases that would be produced in the trial-average ERSP by (here) different motor response latencies across trials with respect to the preceding stimulus onsets. Standardizing response latencies by this means (e.g., aligning the response times to the group-median response latency) also allows averaging across subjects with different reaction time distributions. Note that the latency alignment method can be used to standardize not only the recorded response latencies but also the estimated lags of brain responses captured by, e.g., the lag extraction tool, *pop\_extractlag()* implemented as an EEGLAB plug-in by Gramfort et al. (2010).

Figure 3 demonstrates the procedure of time-warping ERSPs to more than one event in a sequence of events that occurred in each trial. If the peak of the average motor response-locked ERP for an IC, such as that shown as blue trace below the stacked-trials ERP-image plots in Fig. 3a, is as large as or larger than the post-stimulus and stimulus time-locked ERP features, the single-trial ERSPs may need to be time-warped. Accordingly, here a two-sample *t*-test was performed to test the null hypothesis that the observed ERSP peak came from populations with equal means, against the alternative that the means are unequal. In the case that the test rejected the null hypothesis at the default  $\alpha = 0.05$  significance level, single-trial ERSPs were then linearly time-warped so

that the adjusted latency of the button press was the same in each epoch.

In the conventional procedure illustrated in Fig. 3b, the average of the single-trial ERSPs is derived from single-trial data time-locked to imperative stimulus onsets. Since the single-trial ERSP contains features time-locked to the variable-latency subject button press, not to the imperative stimulus, and the button press latencies with respect to stimulus onsets vary widely across trials, near the range of reaction times the average ERSP becomes indistinct and prone to misinterpretation. Fig. 3c shows the response time-warped ERSP derived by warping single-trial ERSPs to be time-locked to both stimulus onsets and to button presses, thereby making the mean ERSP time-locked both to imperative stimulus onsets and button press responses. The time-warped mean ERSP suggests that a near 20-Hz peak in the IC power spectrum begins to emerge *at or just before* the button presses, not well before them as suggested (indistinctly) by the stimulus-locked mean ERSP in Fig. 3b.

***Figure 3. An IC in the rPRECu cluster exhibits a mean ERSP difference before and after time warping to both stimulus onsets and button press responses.***

#### *Multiple-subject IC clustering*

We applied an enhancement of the original Ranking and Averaging Independent Component Analysis by Reproducibility (RAICAR; Yang et al., 2008) clustering approach to both within-subject as well as across-subjects component reproducibility analyses. Figure 4 illustrates the procedure of source imaging, cortical and event-related measure latency alignment, component selection and clustering. To prepare the data for clustering, the spatiotemporal (source-localized ICA or EMSICA) component source distributions were concatenated and then reshaped into a vector. The subject 2-D (latency by frequency) ERSP images were also concatenated and then vectorized. The vectorized ERSP and the IC active source area data were scaled to have equal variance and then stacked to form a single column vector for each IC. The resulting IC column vectors were

concatenated to form a (tall) 2-D matrix of size (rows: #latencies  $\times$  #frequencies  $\times$  #conditions + #vertices on the left and right cortical surface meshes) by (columns) the number of components,  $K$ . The 2-D matrix from the  $S$  runs (for the reproducibility analysis within subjects) or subjects (for reproducibility analysis across subjects) were pooled together to construct a between-runs or between-subjects correlation matrix. The left upper images in Fig. 4c and 4d illustrate the correlation matrix, after rearrangement by RAICAR clustering.

In RAICAR clustering, an IC pair with the highest pairwise similarity is selected to form a cluster, and all the ICs from these two subjects are excluded from the further selection process. The remaining ICs with the highest pairwise similarity to the two selected ICs are grouped into the cluster, this procedure continuing until each subject has one and only one IC selected into the cluster. This clustering procedure is repeated to form more clusters until  $C$  aligned component clusters are identified.

In the original RAICAR approach, a *reproducibility index* for each aligned component is defined by summing the *spatiotemporal correlation coefficients* (SCCs), among the aligned components that are above a specific SCC threshold. As demonstrated by Pendse et al. (2011), RAICAR may use an arbitrary threshold selected "by eye," or may be set to an arbitrary value, such as 50% of the maximum reproducibility value. Meanwhile, the normalized reproducibility obtained by RAICAR may be much lower for between-subjects analysis compared to within-subject analysis (Pendse et al., 2011, Figure 1). Here, we used a simple modification to RAICAR, using the test-retest reproducibility analysis to avoid subjective user decisions but still allowing for threshold optimization.

We defined  $P_R$  as the probability that a truly reliable component is classified as reliable and  $P_U$ , the probability that a truly unreliable component is classified as reliable. In the component selection process, the true status of each component is unknown, but the two proportions can be estimated from SCCs of the aligned components. Genovese et al. (1997) suggested estimating the proportions at a particular threshold by assuming a mixed binomial model underlying the number of times (of  $S$  replications) that a component is consistently classified as reliable. Let  $R_c$  represent the number of replications ( $\leq S$ ) in which a component is classified reliable. Unlike conventional RAICAR, we redefined  $R_c/S$  to be the *reproducibility index* of the  $ct^h$  cluster. In the

reproducibility analysis, the data are assumed to be statistically independent across both components and replications, and each  $R_c$ , is assumed to be a random sample drawn from the mixture of two binomial distributions

$$f(P_R, P_U, \lambda) = \binom{S}{R_c} [\lambda P_R^{R_c} (1 - P_R)^{S - R_c} + (1 - \lambda) P_U^{R_c} (1 - P_U)^{S - R_c}] \quad (8)$$

where  $\lambda$  is the proportion of truly reliable components. Given a SCC threshold, the number of classified reliable component in the  $ct/h$  cluster,  $R_c$ , can be determined, and the likelihood function, the product of (8) for  $C$  aligned components, can be written as,  $l(P_R, P_U, \lambda) = \prod_{c=1}^C f(P_R, P_U, \lambda)$ . This study used a maximum likelihood procedure to estimate parameters  $P_R$ ,  $P_U$  and  $\lambda$  given all possible SCC thresholds, allowing us to plot the Receiver Operating Characteristic (ROC) curve. The operational point on the ROC curve (i.e., the optimal threshold) for classifying components as reliable or unreliable was found by maximizing the *Kappa* value (Cohen, 1960; Liou et al., 2003) defined as

$$Kappa = \frac{P_o - P_c}{1 - P_c} \quad (9)$$

where  $P_o$  is the proportion of correct classifications and  $P_c$ , its expected value. The right upper images in Fig. 4c and 4d show ROC (red) and *Kappa* (green) traces.

**Component selection within subjects** involved IC reproducibility analysis to examine, within subjects, the extent of IC consistency in both cortical location and ERSF features. Similar to most ICA algorithms (see, Himberg et al., 2004; Yang et al., 2008), EMSICA is stochastic, giving slightly different estimates in multiple runs on the same data. To assess the algorithmic reliability of the estimated components, the EMSICA decomposition was run several (here, 25) times using different starting points. ICs with a reproducibility index lower than 75% were then removed. The bar chart at the bottom of Fig. 4c shows the *reproducibility index* of the runs within Subject 1. After algorithmic component reliability analysis for each subject, for each subject about 25 ICs on average for each subject were retained for clustering. Most *unreliable* ICs had “sparse” brain activation patterns and noisy (and on the scalp, relatively small) time courses.

**Component clustering across subjects** was conducted by examining the consistency of spatiotemporal component measures, clustering together ICs from different subjects that were relatively similar to each other by both (cortically co-registered) source location

and (time-warped) ERSP features. Automatic determination of the number of clusters used the results of component reproducibility analysis, as shown in Fig. 4d. Here we retrieved the IC cortical maps that were spatially proximal and moderately reproducible (over 75%) across subjects.

**Figure 4. Multi-subject spatiotemporal cortex- and ERSP latency-aligned IC clustering.**

## Results

Clustering the cortical surface co-registered and motor response latency-aligned EMSICA components produced ten IC clusters. Eight of them are summarized in the panel of the first column in Figure 5 which shows supra-threshold voxel clusters on the cortical surface and cluster-mean time-warped, both stimulus-locked and motor response-locked ERSP images. The ten IC clusters were selected as having relatively large mean intra-cluster distances from one another and for consistency of the ERSP features with activity patterns reported in other auditory/visual stop-signal tasks (Alegre et al., 2004; Aron et al., 2004; Knyazev et al., 2008; Savostyanov et al., 2009). For comparison, the corresponding IC clusters obtained by grouping the ICs prior to spatial and temporal alignment, and by the conventional two-stage ICA approach using LORETA, with and without cortical-surface and ERSP-latency alignment, are shown in the 2<sup>nd</sup>, 3<sup>rd</sup>, and 4<sup>th</sup> columns, respectively.

In Fig. 5a (top row), trial by trial ERSP images in the ‘stop’ condition are plotted next to the cortical activation maps. The left *pars opercularis* cluster (*IPOPE $\theta$* ) comprising the posterior region of Broca's area on average exhibited strong theta band excitation following stimulus onsets. This active area appeared in each cluster IC from all 11 subjects. Region 1A (Fig. 5a, 1<sup>st</sup> column: EMSICA results with alignment,) had a more compact spatial distribution than Region 1B in the results of EMSICA without alignment (1<sup>st</sup> row, 2<sup>nd</sup> column). Similarly, the period of alpha-band (*mu*) suppression labeled 1C in the time-warped ERSP image (1<sup>st</sup> column) is briefer than Region 1D in the not time-

warped ERSP (2<sup>nd</sup> column). Inspection of individual member components of this cluster showed this duration difference to be consistent across subjects.

The second cluster is associated with voxels in the anterior cingulate cortex ( $ACC\theta$  in Fig. 5b). Comparing the areas labeled 2A, 2B, 2C, and 2D, the cortex- and latency-based aligned EMSICA results again exhibit more compact spatial/temporal distributions.

The right inferior frontal cluster ( $rIFC\theta$  in Fig. 5c) is associated with voxels in right *pars opercularis*, *pars triangularis*, and *pars orbitalis*. At least nine member components show right lateralization with high z-values. Although the activity in area 3B in the unaligned data labeled (2<sup>nd</sup> column) appears to be more compact than in region 3A in the aligned data (1<sup>st</sup> column), the cluster quality index (described below) is actually lower. Furthermore, theta synchronization in this area (feature 3D, unaligned data) seems to be not so pronounced as that in 3C (aligned data).

***Figure 5. Eight spatiotemporal component clusters of interest.***

The fourth cluster shown ( $lIPp300$  in Figure 5d) has supra-threshold voxels in the left inferior parietal that exhibit a late positive-going response complex (P300) in the ERP as well as a low-frequency power increase following stimulus onset. This cluster appears to sum similar event-related activity patterns occurring in several brain areas of inferior parietal cortex. The ERSP images in the ‘press’ condition are plotted next to the cortical activation maps. The low-frequency excitation is clearly weaker in the two-stage cluster data (features 4B and 4C) than in the cortex- and latency-aligned EMSICA results (feature 4A).

The left precentral and postcentral component clusters ( $lPREC\mu$  and  $lPSTS\mu$ ; Fig. 5e-5f) exhibit the defining feature of *mu* rhythms (Babiloni et al., 1999; Cochin et al., 1998) — characteristic spectral peaks near 11 Hz and 22 Hz that are strongly attenuated before and/or after movements. Right precentral and postcentral *mu* rhythm component clusters (clusters  $rPREC\mu$  and  $rPSTS\mu$ , not shown) with similar *mu* blocking and weaker beta

rebound peaks were also found by EMSICA clustering. The beta band rebound peak is more pronounced in the motor response-aligned data results (ERSP Features 6B and 6E) than in the unaligned data results (Features 6C and 6F).

Further, the active area for  $lPSTS\mu$  obtained using EMSICA (Region 6A) appears to be in or near hand-related postcentral somatosensory cortex, while Region 6D obtained in the two-stage ICA source imaging approach is shifted to (or near) the lower face area, suggesting that clustering EMSICA components with alignment can obtain more precise activation regions.

The active areas of the occipital alpha-rhythm component clusters ( $lLOCC\alpha$  and  $rLOCC\alpha$  in Fig. 5g-5h) are in the left and right occipital regions. This active area obtained using EMSICA with alignment (Fig. 5g-5h, 1<sup>st</sup> column) appears to have a more compact spatial distribution than for EMSICA without alignment, including voxels in temporal cortex (2<sup>nd</sup> column, Regions 7C and 8C). The latency-aligned EMSICA components were also time-warped to the subject motor response. Comparing Regions 7A with 7C, 7B with 7D, 8A with 8C, and 8B with 8D, the surface- and latency-aligned EMSICA components appear to exhibit more compact spatial/temporal features.

Figure 5 also shows that counterparts of some EMSICA clusters are missing in the results of the two-stage approach (e.g., the  $lPOPE\theta$  and  $lPREC\mu$  clusters). To further characterize the compactness of each cluster in terms of its active cortical topography and its ERSP image, we computed the cluster quality index defined by (Himberg et al., 2004) as

$$q_k = \frac{1}{|C_k|^2} \sum_{i,j \in C_k} |r_{ij}| \quad (10)$$

where  $|r_{ij}|$  is the absolute value of the correlation coefficients between component members  $i$  and  $j$ , whereas  $C_k$  is the set of indices belonging to the  $k$ th cluster, and  $|C_k|$  is the size of the  $k$ th cluster. Figure 6 gives a summary of cluster quality indices listed according to active cortical areas (Fig. 6a) and ERSP images (Fig. 6b), respectively, for each component cluster. For all clusters, and by both ERSP image and active cortical area correlations EMSICA components produced, on average, higher cluster quality indices.

*Figure 6. Compactness of clusters summarizing similarities for all component pairs in each of the eight clusters.*

## Discussion and Conclusions

Conventional ICA decomposition of EEG and MEG data first separate the component time courses then locate the cortical origins of the separated components. This approach is viable for group analysis because source dipole probability distributions can be estimated by equivalent single dipole (or on occasion symmetric dual-dipole) models of individual component source distributions (Delorme et al., 2012; Onton et al., 2005). This study proposes a further group analysis step based on unified spatiotemporal ICA decomposition, spatial cortical model alignment and temporal event latency alignment, and uses this approach to explore consistent EEG source dynamics from eleven subjects performing a stop-signal task.

The group analysis found ten clusters ( $lPOPE\theta$ ,  $ACC\theta$ ,  $rIFC\theta$ ,  $lPp300$ ,  $l/rPREC\mu$ ,  $l/rPSTS\mu$ , and  $l/rLOCC\alpha$ ) of spatiotemporal ICA component processes involved in the inhibition and performance-monitoring task: Knyazev et al. (2010) showed that reciprocal relationships between anterior slow-wave (delta and theta) and posterior alpha activity reflect interaction of activation and inhibition during behavior regulation. Here, the active area of the  $lPOPE\theta$  cluster is consistent with studies reported an association between the ventrolateral prefrontal cortex (VLPFC) and maintenance of rules involving item properties (Aron et al., 2004; Christoff and Keramatian, 2007; Garavan et al., 2002).

According to horse-race model (Band et al., 2003), anterior cortex (frontal areas and anterior cingulate) is an area of competition between activating and inhibitory processes. Many neuroimaging studies have demonstrated that the anterior cingulate cortex (ACC) is engaged in detecting or dealing with conflict between a stop signal and an intended action (Gehring and Knight, 2000), and that, subsequently, right inferior frontal cortex ( $rIFC$ ) is involved in suppressing the intended response (Aron et al., 2004), supporting the findings of the involvement of  $ACC\theta$  and  $rIFC\theta$  in these data. The neurophysiological functions of the source clusters for this stop signal task are worth

further exploration to better understand the hierarchy of inhibitory processes (see Huster et al., 2013 for a review). For example, the association of beta oscillations in and coherence between the *rIFC* and pre-supplementary motor areas associated with inhibitory control has also become a focus of attention in this task context (Aron, 2011; Swann et al., 2009; Swann et al., 2012).

As shown in Fig. 5(a-c, e-h) when single-trial ERSPs are time-warped to produce fixed latencies of each of a sequence of experimental trial events (here, stimulus onsets and ensuing stop signals, Fig. 5a-5c, or subject button presses, Fig. 5e-5h), the spectral modulation of different frequency bands associated with specific aspects of the events becomes more precise and pronounced.

The left precentral and postcentral *mu* rhythm (*IPREC $\mu$*  and *IPSTS $\mu$* ) clusters located in or near right-hand somatomotor cortex exhibited near 10-Hz and 20-Hz spectral peaks that were, as expected, blocked when subjects performed motor responses. In addition, power near 20 Hz showed a more pronounced and earlier rebound following the motor response than power near 10 Hz, especially in the precentral cortex (Hari, 2006; Nagamine et al., 1996; Pfurtscheller, 1981; Salmelin and Hari, 1994). Figure 5e shows a clearer termination of alpha desynchronization before movement and beta rebound after movement in the spatially and temporally aligned EMSICA components than in the temporally nonaligned components. In general, latency alignment increased the amplitude of the event-related theta bursts in the left and right *LOCC $\alpha$*  clusters, the 20-Hz increase in the *IPREC $\mu$*  and *IPSTS $\mu$*  clusters following the motor response, and the theta-band increase in the *ACC $\theta$*  cluster following the Stop signal. All these sensorimotor brain areas are known to be involved in human perception of, reaction to, and interactions with the external environment.

The time-warping method was originally proposed in (Makeig et al., 2007) and was applied in (Gwin et al., 2011). This study enhanced this method by introducing a two-sample t-test procedure to automatically determine whether the component needs to be time-warped or not. It has been shown that ICA component processes can exhibit both stimulus- and response-locked response features. However, these mostly occur in mostly separate classes of independent components (Jung et al., 2001). Here, the numbers of components in each class varied between subjects. In these data, about 10 of 25

components on average for each subject, retained for clustering by IC reproducibility analysis, had significant two-sample t-test values at response-locked (in the ‘press’ condition) ERP peaks and 5 components had significant values at stop-signal locked peaks (in the ‘stop’ condition).

This procedure for detecting components with response-locked activities is demonstrated in Fig. 3. By performing a similar procedure on the stimulus-locked peaks, we found about 15 components to have stimulus-locked activity peaks. Our results for each subject also found that a few component activities had ERP peaks time-locked to both stimulus presentations and button presses. The linear time-warping procedure was also applied to single-trial ERSPs for these components, since the procedure ensured that time-locked responses to both events of interest (stimulus onsets and participant responses) were latency aligned across trials. Because homogeneity of an IC cluster is most accurately assessed and characterized by the activities of its constituent ICs, those identified event-related activity patterns may also provide auxiliary information useful for obtaining functionally consistent clusters.

While ERSP latency alignment by time-warping allows better visualization of spectral perturbations time-locked to a sequence of two (or more) trial events with varying inter-event latencies, cortical surface-based alignment of active source areas enables multi-subject analysis that takes into account inter-subject cortical surface variability. The now conventional approach to EEG source localization performs inverse modeling of EEG current dipole/density source distributions in an individual or template 3-D head model, e.g., using a boundary element method (BEM) forward head model based on an MNI head template based on a large number of MRI head images. The cortical alignment procedure demonstrated here localizes sources on a high-resolution individual cortical surface model for each subject, then maps the individually-aligned cortical source areas onto a template cortical hemisphere computed from the individual cortical hemisphere models of all the subjects.

Here, the precentral and postcentral *mu* rhythm (*IPREC $\mu$*  and *IPSTS $\mu$* ) clusters found by single spatiotemporal ICA decomposition (Fig. 5e-5f, columns 1 and 2) were merged into a single component cluster by the two-stage ICA approach (columns 3 and 4).

Inspection of nonaligned individual maps in each cluster suggested a large variation among locations of the most active voxels. The proposed corticospatial and latency alignment approach thus might offer more meaningful component clusters that are more spatially compact and have more distinct event-related spectral dynamics (Fig. 6, Column 1 versus the others).

ICA approaches take advantage of the high temporal resolution of EEG imaging to directly examine the brain dynamics of cortical component processes including their event-related spectral perturbations that, as here, may have a duration of 2 s or more following meaningful task events. Most psychophysiological source analysis studies, however, have performed inverse solutions only on ERP peak latencies (e.g., in the latency range including the P1, P2, P300, N400 ERP peaks). Studies applying ICA to individual subject data have found that time courses of average ERPs in cognitive tasks are generated by multiple, spatially-distributed sources with overlapping scalp topographies (Makeig et al., 2004; Makeig et al., 2002; Moores et al., 2003). Performing ICA decomposition of the single-trial or continuous EEG data to separate the data into temporally independent components, and then performing source localization *post hoc* may thus give more useful information about cortical function than conventional ERP peak localization. However, because of inadequacy of template head models and between-subject differences in cortical geometry, ICA-based two-stage source analysis estimated from each IC's scalp map may not yield precise and spatially distinct clusters of response generators. The EMSICA single-stage decomposition approach demonstrated here may potentially more clearly separate EEG data into a sum of cortical source activities.

The approach taken in this study takes into account substantial inter-subject cortical and latency variations while identifying clusters of EEG sources, co-registered to the cortical surface and in common across a group of subjects. Here, for both the extended infomax ICA and EMSICA decomposition approaches, aligning component active cortical topographies and single-trial ERSP image events not only helped reduce inter-subject variability in cortical areas and event-related responses, but also facilitated identification and visualization of spatially, temporally, and functionally equivalent IC processes across subjects. Because of this, the proposed spatiotemporal independent

source imaging and clustering approach may be more accurate than existing source-localization methods. Comparing cortical surface-clustered ICA and EMSICA results in Figure 6 gave some (weak) evidence that EMSICA may deliver better results than extended infomax ICA. However, a more detailed statistical comparison at the single-subject level would be required to answer this question.

To more precisely localize and identify the source distributions, a whole-head structural MR image of each subject can be used to build a high-quality BEM or finite element method (FEM) head model for each subject, and to co-register these with the known or recorded electrode positions and thereby compute accurate lead field matrices (Akalin Acar and Makeig, 2010, 2013). In this paper, we assumed homogeneous isotropic conductivities of 0.33, 1, 0.0042, and 0.33 ( $\Omega m$ )<sup>-1</sup> for brain, CSF, skull, and scalp, respectively (Mosher et al., 1993). The skull conductivity was used as 1/80 as compared with brain conductivity. The issue of brain-to-skull conductivity ratio has recently drawn attention in biophysics research of the brain. For example, Akalin Acar and Makeig (2013) and Wang and Ren (2013) have demonstrated that correct modeling of skull conductivity is an important factor for EEG source localization, quite possibly outweighing the choice of head model. In future work we should consider the effects of skull conductivity on EMSICA results.

Chief among the problems introduced by spatiotemporal independent EEG source imaging is the issue of how to cluster ICs across subjects. It is worth discussing some alternatives to spatiotemporal component clustering to define clusters that represent common EEG activities across subjects. This study applied a modified RAICAR procedure using the test-retest reproducibility analysis for threshold optimization to select acceptable clusters and their components. The matching procedure in RAICAR, however, forces every subject to contribute exactly one component to each cluster. Though here, the SCC threshold was determined *post hoc* and therefore some or all clusters may not have included contributions from all subjects, those excluded components did not have any chance to become members of other clusters. To address this problem, during the matching procedure components whose average correlation values with other components are lower than the threshold (and thus are excluded from the cluster) are

allowed to be candidates for other clusters. Here again, the threshold might be determined using test-retest reproducibility analysis.

Though the preliminary multiple-subject IC clustering strategy presented in this article demonstrates some of the basic capabilities of the proposed analysis procedure, some issues, for example, how to balance between the correlation matrix of measures still need to be explored. Here, the ERSP images and active source area data were concatenated to form a single vector and correlation matrix. One might also introduce weights on the temporal and spatial correlation matrices to balance between them (Esposito et al., 2005). These weights could depend on the task performed or on other factors (Kherif et al., 2003). An extension of the Measure Projection clustering approach of Bigdely-Shamlo et al. (2013) to the flattened, co-registered cortical surface might also be of interest.

A further step in group analysis may be to cluster component processes on other measures of EEG dynamics, such as inter-trial phase coupling (Makeig et al., 2004; Sauseng et al., 2008), phase-amplitude coupling (Tort et al., 2010), component cross-coherence, and/or source information flow measures (Mullen et al., 2010; Supp et al., 2007). Incorporating more EEG dynamics may produce component clusters that are more neurophysiologically robust. However, it is also possible that the spatial boundaries of clusters of similar component processes may not be the same for different measures (Bigdely-Shamlo et al., 2013; Onton and Makeig, 2006).

We recognize that for many EEG studies the expense of MR imaging and/or its requirement that the subject lie still during the scan may not make analysis using individual MR head images possible. We believe, however, that when possible, using cortically aligned spatial head models and event-aligned component process measures may represent another step toward the long-elusive goal of achieving both high spatial and temporal resolution in EEG imaging, an accomplishment that could bring EEG once again to the forefront of human neuroscience research.

## **Acknowledgments**

The authors are indebted to Professor Chia-Ying Lee for helping develop strategies for successful EEG data collection and to Alejandro Ojeda Gonzalez for helpful discussions on the LORETA algorithm. This research was supported by grants NSC96-2413-H-001-001-MY3 from the National Science Council, Taiwan, by the US Office of Naval Research, the Army Research Office (W911NF-09-1-0510), the Army Research Laboratory (W911NF-10-2-0022), and DARPA (DARPA/USDI D11PC20183), and by a gift from The Swartz Foundation (Old Field NY).

## References

- Akalin Acar, Z., Makeig, S., 2010. Neuroelectromagnetic Forward Head Modeling Toolbox. *J. Neurosci. Meth.* 190, 258-270.
- Alegre, M., Gurtubay, I.G., Labarga, A., Iriarte, J., Valencia, M., Artieda, J., 2004. Frontal and central oscillatory changes related to different aspects of the motor process: a study in go/no-go paradigms. *Exp. Brain. Res.* 159, 14-22.
- Aron, A.R., 2011. From reactive to proactive and selective control: developing a richer model for stopping inappropriate responses. *Biol Psychiatry* 69, e55-68.
- Aron, A.R., Robbins, T.W., Poldrack, R.A., 2004. Inhibition and the right inferior frontal cortex. *Trends. Cogn. Sci.* 8, 170-177.
- Babiloni, C., Carducci, F., Cincotti, F., Rossini, P.M., Neuper, C., Pfurtscheller, G., Babiloni, F., 1999. Human movement-related potentials vs desynchronization of EEG alpha rhythm: A high-resolution EEG study. *NeuroImage* 10, 658-665.
- Baillet, S., Mosher, J.C., Leahy, R.M., 2001. Electromagnetic brain mapping. *IEEE Signal Proc. Mag.* 18, 14-30.
- Band, G.P.H., van der Molen, M.W., Logan, G.D., 2003. Horse-race model simulations of the stop-signal procedure. *Acta Psychol.* 112, 105-142.
- Beckmann, C.F., Smith, S.A., 2004. Probabilistic independent component analysis for functional magnetic resonance imaging. *IEEE Trans. Med. Imaging* 23, 137-152.
- Bigdely-Shamlo, N., Mullen, T., Kreutz-Delgado, K., Makeig, S., 2013. Measure projection analysis: a probabilistic approach to EEG source comparison and multi-subject inference. *Neuroimage* 72, 287-303.
- Calhoun, V.D., Liu, J., Adali, T., 2009. A review of group ICA for fMRI data and ICA for joint inference of imaging, genetic, and ERP data. *NeuroImage* 45, S163-S172.
- Christoff, K., Keramatian, K., 2007. Abstraction of Mental Representations: Theoretical Considerations and Neuroscientific Evidence. In: Bunge, S.A., Wallis, J.D. (Eds.), *Neuroscience of rule-guided behavior*, pp. 107-126.
- Cochin, S., Barthelemy, C., Lejeune, B., Roux, S., Martineau, J., 1998. Perception of motion and qEEG activity in human adults. *Electroen. Clin. Neuro.* 107, 287-295.
- Cohen, J., 1960. A Coefficient of Agreement for Nominal Scales. *Educ. Psychol. Meas.* 20, 37-46.
- Congedo, M., John, R.E., De Ridder, D., Prichep, L., 2010. Group independent component analysis of resting state EEG in large normative samples. *Int. J. Psychophysiol.* 78, 89-99.
- Dale, A.M., Fischl, B., Sereno, M.I., 1999. Cortical surface-based analysis - I. Segmentation and surface reconstruction. *NeuroImage* 9, 179-194.
- De Lucia, M., Michel, C.M., Murray, M.M., 2010. Comparing ICA-based and Single-Trial Topographic ERP Analyses. *Brain Topogr.* 23, 119-127.
- Delorme, A., Makeig, S., 2004. EEGLAB: an open source toolbox for analysis of single-trial EEG dynamics including independent component analysis. *J. Neurosci. Meth.* 134, 9-21.
- Delorme, A., Palmer, J., Onton, J., Oostenveld, R., Makeig, S., 2012. Independent EEG Sources Are Dipolar. *Plos One* 7.
- Delorme, A., Westerfield, M., Makeig, S., 2007. Medial prefrontal theta bursts precede rapid motor responses during visual selective attention. *J Neurosci.* 27, 11949-11959.
- Desikan, R.S., Segonne, F., Fischl, B., Quinn, B.T., Dickerson, B.C., Blacker, D., Buckner, R.L., Dale, A.M., Maguire, R.P., Hyman, B.T., Albert, M.S., Killiany, R.J., 2006. An automated labeling system for subdividing the human cerebral cortex on MRI scans into gyral based regions of interest. *Neuroimage* 31, 968-980.
- Destrieux, C., Fischl, B., Dale, A., Halgren, E., 2010. Automatic parcellation of human cortical gyri and sulci using standard anatomical nomenclature. *Neuroimage* 53, 1-15.
- Eichele, T., Calhoun, V.D., Debener, S., 2009. Mining EEG-fMRI using independent component analysis. *Int. J. Psychophysiol.* 73, 53-61.

- Eichele, T., Calhoun, V.D., Moosmann, M., Specht, K., Jongsma, M.L.A., Quiroga, R.Q., Nordby, H., Hugdahl, K., 2008. Unmixing concurrent EEG-fMRI with parallel independent component analysis. *Int. J. Psychophysiol.* 67, 222-234.
- Esposito, F., Scarabino, T., Hyvarinen, A., Himberg, J., Formisano, E., Comani, S., Tedeschi, G., Goebel, R., Seifritz, E., Di Salle, F., 2005. Independent component analysis of fMRI group studies by self-organizing clustering. *NeuroImage* 25, 193-205.
- Fischl, B., Sereno, M.I., Tootell, R.B.H., Dale, A.M., 1999. High-resolution intersubject averaging and a coordinate system for the cortical surface. *Hum. Brain Mapp.* 8, 272-284.
- Garavan, H., Ross, T.J., Murphy, K., Roche, R.A.P., Stein, E.A., 2002. Dissociable executive functions in the dynamic control of behavior: Inhibition, error detection, and correction. *NeuroImage* 17, 1820-1829.
- Gehring, W.J., Knight, R.T., 2000. Prefrontal-cingulate interactions in action monitoring. *Nat. Neurosci.* 3, 516-520.
- Genovese, C.R., Noll, D.C., Eddy, W.F., 1997. Estimating test-retest reliability in functional MR imaging. I: Statistical methodology. *Magn. Reson. Med.* 38, 497-507.
- Gramfort, A., Keriven, R., Clerc, M., 2010. Graph-Based Variability Estimation in Single-Trial Event-Related Neural Responses. *IEEE Trans. Biomed. Eng.* 57, 1051-1061.
- Gwin, J.T., Gramann, K., Makeig, S., Ferris, D.P., 2011. Electrocortical activity is coupled to gait cycle phase during treadmill walking. *Neuroimage* 54, 1289-1296.
- Hämäläinen, M.S., 2009. MNE Software. Downloaded from: <http://martinos.org/mne/>.
- Hämäläinen, M.S., Ilmoniemi, R.J., 1994. Interpreting Magnetic-Fields of the Brain - Minimum Norm Estimates. *Med. Biol. Eng. Comput.* 32, 35-42.
- Hari, R., 2006. Action-perception connection and the cortical mu rhythm. In: Neuper, C., Klimesch, W. (Eds.), *Event-Related Dynamics of Brain Oscillations*. Amsterdam: Elsevier, pp. 253-260.
- Himberg, J., Hyvarinen, A., Esposito, F., 2004. Validating the independent components of neuroimaging time series via clustering and visualization. *NeuroImage* 22, 1214-1222.
- Huang, H.C., Jansen, B.H., 1985. EEG waveform analysis by means of dynamic time-warping. *Int. J. Biomed. Comput.* 17, 135-144.
- Huster, R.J., Enriquez-Geppert, S., Lavallee, C.F., Falkenstein, M., Herrmann, C.S., 2013. Electroencephalography of response inhibition tasks: functional networks and cognitive contributions. *Int J Psychophysiol* 87, 217-233.
- Hyvärinen, A., 1999. Fast and robust fixed-point algorithms for independent component analysis. *IEEE Trans. Neural Networ.* 10, 626-634.
- Jenkinson, M., Pechaud, M., Smith, S., 2005. BET2: MR-Based Estimation of Brain, Skull and Scalp Surfaces. Eleventh Annual Meeting of the Organization for Human Brain Mapping.
- Jung, T.P., Makeig, S., Westerfield, M., Townsend, J., Courchesne, E., Sejnowski, T.J., 2001. Analysis and visualization of single-trial event-related potentials. *Hum. Brain Mapp.* 14, 166-185.
- Kherif, F., Poline, J.B., Meriaux, S., Benali, H., Flandin, G., Brett, M., 2003. Group analysis in functional neuroimaging: selecting subjects using similarity measures. *Neuroimage* 20, 2197-2208.
- Klopp, J., Marinkovic, K., Chauvel, P., Nenov, V., Halgren, E., 2000. Early widespread cortical distribution of coherent fusiform face selective activity. *Hum. Brain Mapp.* 11, 286-293.
- Knyazev, G.G., Levin, E.A., Savostyanov, A.N., 2008. A failure to stop and attention fluctuations: An evoked oscillations study of the stop-signal paradigm. *Clin. Neurophysiol.* 119, 556-567.
- Knyazev, G.G., Slobodskoi-Plyusnin, Y.Y., Savostyanov, A.N., Levin, E.A., Bocharov, A.V., 2010. Reciprocal Relationships Between the Oscillatory Systems of the Brain. *Neurosci. Behav. Physi.* 40, 29-35.

- Knyazev, G.G., Slobodskoj-Plusnin, J.Y., Bocharov, A.V., Pylkova, L.V., 2011. The default mode network and EEG alpha oscillations: An independent component analysis. *Brain Res.* 1402, 67-79.
- Kovacevic, N., McIntosh, A.R., 2007. Groupwise independent component decomposition of EEG data and partial least square analysis. *NeuroImage* 35, 1103-1112.
- Langers, D.R.M., 2010. Unbiased Group-Level Statistical Assessment of Independent Component Maps by Means of Automated Retrospective Matching. *Hum. Brain Mapp.* 31, 727-742.
- Lee, T.W., Girolami, M., Sejnowski, T.J., 1999. Independent component analysis using an extended infomax algorithm for mixed subgaussian and supergaussian sources. *Neural Comput.* 11, 417-441.
- Liou, M., Su, H.R., Lee, J.D., Cheng, P.E., Huang, C.C., Tsai, C.H., 2003. Bridging functional MR images and scientific inference: Reproducibility maps. *J. Cognitive Neurosci.* 15, 935-945.
- Logan, G.D., Cowan, W.B., Davis, K.A., 1984. On the Ability to Inhibit Simple and Choice Reaction-Time Responses - a Model and a Method. *J. Exp. Psychol. Hum. Percept. Perform.* 10, 276-291.
- Maintz, J.B.A., Viergever, M.A., 1998. A survey of medical image registration. *Med. Image Anal.* 2, 1-36.
- Makeig, S., 1993. Auditory Event-Related Dynamics of the Eeg Spectrum and Effects of Exposure to Tones. *Electroen. Clin. Neuro.* 86, 283-293.
- Makeig, S., Bell, A.J., Jung, T.P., Sejnowski, T.J., 1996. Independent component analysis of electroencephalographic data. *Adv. Neural Inf. Process Syst.* 8, 145-151.
- Makeig, S., Delorme, A., Westerfield, M., Jung, T.-P., Townsend, J., Courchesne, E., Sejnowski, T.J., 2004. Electroencephalographic Brain Dynamics Following Manually Responded Visual Targets. *PLoS Biol.* 2, e176.
- Makeig, S., Jung, T.P., Bell, A.J., Ghahremani, D., Sejnowski, T.J., 1997. Blind separation of auditory event-related brain responses into independent components. *Proc. Natl. Acad. Sci. U. S. A.* 94, 10979-10984.
- Makeig, S., Onton, J., Sejnowski, T., Poizner, H., 2007. Prospects for mobile, high-definition brain imaging: spectral modulations during 3-D reaching. *Hum. Brain Mapp. Chicago, IL.*
- Makeig, S., Westerfield, M., Jung, T.P., Enghoff, S., Townsend, J., Courchesne, E., Sejnowski, T.J., 2002. Dynamic brain sources of visual evoked responses. *Science* 295, 690-694.
- Marco-Pallarés, J., Grau, C., Ruffini, G., 2005. Combined ICA-LORETA analysis of mismatch negativity. *NeuroImage* 25, 471-477.
- McKeown, M., Makeig, S., Brown, G., Jung, T.-P., Kindermann, S., Bell, A., Sejnowski, T., 1998. Analysis of fMRI Data by Blind Separation Into Independent Spatial Components. *Hum. Brain Mapp.* 6, 160-188.
- Milne, E., Scope, A., Pascalis, O., Buckley, D., Makeig, S., 2009. Independent Component Analysis Reveals Atypical Electroencephalographic Activity During Visual Perception in Individuals with Autism. *Biol. Psychiat.* 65, 22-30.
- Moores, K.A., Clark, C.R., Hadfield, J.L.M., Brown, G.C., Taylor, D.J., Fitzgibbon, S.P., Lewis, A.C., Weber, D.L., Greenblatt, R., 2003. Investigating the generators of the scalp recorded visuo-verbal P300 using cortically constrained source localization. *Hum. Brain Mapp.* 18, 53-77.
- Mosher, J.C., Lewis, P.S., Leahy, R.M., 1992. Multiple dipole modeling and localization from spatio-temporal MEG data. *IEEE Trans. Biomed. Eng.* 39, 541-557.
- Mosher, J.C., Spencer, M.E., Leahy, R.M., Lewis, P.S., 1993. Error-Bounds for Eeg and Meg Dipole Source Localization. *Electroen. Clin. Neuro.* 86, 303-321.
- Mullen, T., Delorme, A., Kothe, C., Makeig, S., 2010. An Electrophysiological Information Flow Toolbox for EEGLAB. Society for Neuroscience Conference, San Diego, CA, USA.

- Nagamine, T., Kajola, M., Salmelin, R., Shibasaki, H., Hari, R., 1996. Movement-related slow cortical magnetic fields and changes of spontaneous MEG- and EEG-brain rhythms. *Electroen. Clin. Neuro.* 99, 274-286.
- Onton, J., Delorme, A., Makeig, S., 2005. Frontal midline EEG dynamics during working memory. *NeuroImage* 27, 341-356.
- Onton, J., Makeig, S., 2006. Information-based modeling of event-related brain dynamics. In: Neuper, C., Klimesch, W. (Eds.), *Event-Related Dynamics of Brain Oscillations*. Amsterdam: Elsevier, pp. 99-120.
- Oostenveld, R., Oostendorp, T.F., 2002. Validating the boundary element method for forward and inverse EEG computations in the presence of a hole in the skull. *Hum. Brain Mapp.* 17, 179-192.
- Pascual-Marqui, R.D., 2002. Standardized low-resolution brain electromagnetic tomography (sLORETA): Technical details. *Method Find Exp. Clin.* 24, 5-12.
- Pascual-Marqui, R.D., Lehmann, D., Koenig, T., Kochi, K., Merlo, M.C.G., Hell, D., Koukkou, M., 1999. Low resolution brain electromagnetic tomography (LORETA) functional imaging in acute, neuroleptic-naive, first-episode, productive schizophrenia. *Psychiat. Res.-Neuroim.* 90, 169-179.
- Pendse, G.V., Borsook, D., Becerra, L., 2011. A simple and objective method for reproducible resting state network (RSN) detection in fMRI. *PLoS One* 6, e27594.
- Pfurtscheller, G., 1981. Central Beta-Rhythm during Sensorimotor Activities in Man. *Electroen. Clin. Neuro.* 51, 253-264.
- Picton, T., Hunt, M., Mowrey, R., Rodriguez, R., Maru, J., 1988. Evaluation of brain-stem auditory evoked potentials using dynamic time warping. *Electroencephalogr. Clin. Neurophysiol.* 71, 212-225.
- Pockett, S., Whalen, S., McPhail, A.V.H., Freeman, W.J., 2007. Topography, independent component analysis and dipole source analysis of movement related potentials. *Cogn. Neurodynamics* 1, 327-340.
- Ponomarev, V.A., Gurskaya, O.E., Kropotov, Y.D., Artjushkova, L.V., Müller, A., 2010. Comparison of methods for clustering independent EEG components in healthy subjects and patients with postconcussion syndrome after traumatic brain injury. *Hum. Physiol.* 36, 123-131.
- Roberts, K., Lawrence, P., Eisen, A., Hoirch, M., 1987. Enhancement and dynamic time warping of somatosensory evoked potential components applied to patients with multiple sclerosis. *IEEE Trans. Biomed. Eng.* 34, 397-405.
- Salmelin, R., Hari, R., 1994. Spatiotemporal characteristics of sensorimotor neuromagnetic rhythms related to thumb movement. *Neuroscience* 60, 537-550.
- Sauseng, P., Klimesch, W., Gruber, W.R., Birbaumer, N., 2008. Cross-frequency phase synchronization: A brain mechanism of memory matching and attention. *NeuroImage* 40, 308-317.
- Savostyanov, A.N., Tsai, A.C., Liou, M., Levin, E.A., Lee, J.D., Yurganov, A.V., Knyazev, G.G., 2009. EEG-correlates of trait anxiety in the stop-signal paradigm. *Neurosci. Lett.* 449, 112-116.
- Scherg, M., Von Cramon, D., 1985. Two bilateral sources of the late AEP as identified by a spatio-temporal dipole model. *Electroencephalogr. Clin. Neurophysiol. Evoked Potentials Section* 62, 32-44.
- Scherg, M., Voncramon, D., 1986. Evoked Dipole Source Potentials of the Human Auditory-Cortex. *Electroencephalogr. Clin. Neurophysiol.* 65, 344-360.
- Smith, S.M., 2002. Fast robust automated brain extraction. *Hum. Brain Mapp.* 17, 143-155.
- Supp, G.G., Schlogl, A., Trujillo-Barreto, N., Muller, M.M., Gruber, T., 2007. Directed Cortical Information Flow during Human Object Recognition: Analyzing Induced EEG Gamma-Band Responses in Brain's Source Space. *Plos One* 2.

- Swann, N., Tandon, N., Canolty, R., Ellmore, T.M., McEvoy, L.K., Dreyer, S., DiSano, M., Aron, A.R., 2009. Intracranial EEG reveals a time- and frequency-specific role for the right inferior frontal gyrus and primary motor cortex in stopping initiated responses. *J Neurosci* 29, 12675-12685.
- Swann, N.C., Cai, W., Conner, C.R., Pieters, T.A., Claffey, M.P., George, J.S., Aron, A.R., Tandon, N., 2012. Roles for the pre-supplementary motor area and the right inferior frontal gyrus in stopping action: electrophysiological responses and functional and structural connectivity. *Neuroimage* 59, 2860-2870.
- Talairach, J., 1967. Atlas d'anatomie stéréotaxique du télencéphale: études anatomo-radiologiques. Masson et Cie.
- Talairach, J., Tournoux, P., 1988. Co-Planar Stereotaxic Atlas of the Human Brain: 3-D Proportional System: An Approach to Cerebral Imaging (Thieme Classics). Thieme.
- Tort, A.B.L., Komorowski, R., Eichenbaum, H., Kopell, N., 2010. Measuring Phase-Amplitude Coupling Between Neuronal Oscillations of Different Frequencies. *J. Neurophysiol.* 104, 1195-1210.
- Tsai, A.C., Liou, M., Jung, T.P., Onton, J.A., Cheng, P.E., Huang, C.C., Duann, J.R., Makeig, S., 2006. Mapping single-trial EEG records on the cortical surface through a spatiotemporal modality. *NeuroImage* 32, 195-207.
- Vakorin, V.A., Kovacevic, N., McIntosh, A.R., 2010. Exploring transient transfer entropy based on a group-wise ICA decomposition of EEG data. *NeuroImage* 49, 1593-1600.
- Wang, G., Ren, D., 2013. Effect of brain-to-skull conductivity ratio on EEG source localization accuracy. *Biomed Res Int*, doi:10.1155/2013/459346.
- Wang, K., Begleiter, H., Porjesz, B., 2001. Warp-averaging event-related potentials. *Clin. Neurophysiol.* 112, 1917-1924.
- Yang, Z., LaConte, S., Weng, X.C., Hu, X.P., 2008. Ranking and averaging independent component analysis by reproducibility (RAICAR). *Hum. Brain Mapp.* 29, 711-725.
- Zhukov, L., Weinstein, D., Johnson, C., 2000. Independent component analysis for EEG source localization. *IEEE Eng. Med. Biol. Mag.* 19, 87-96.

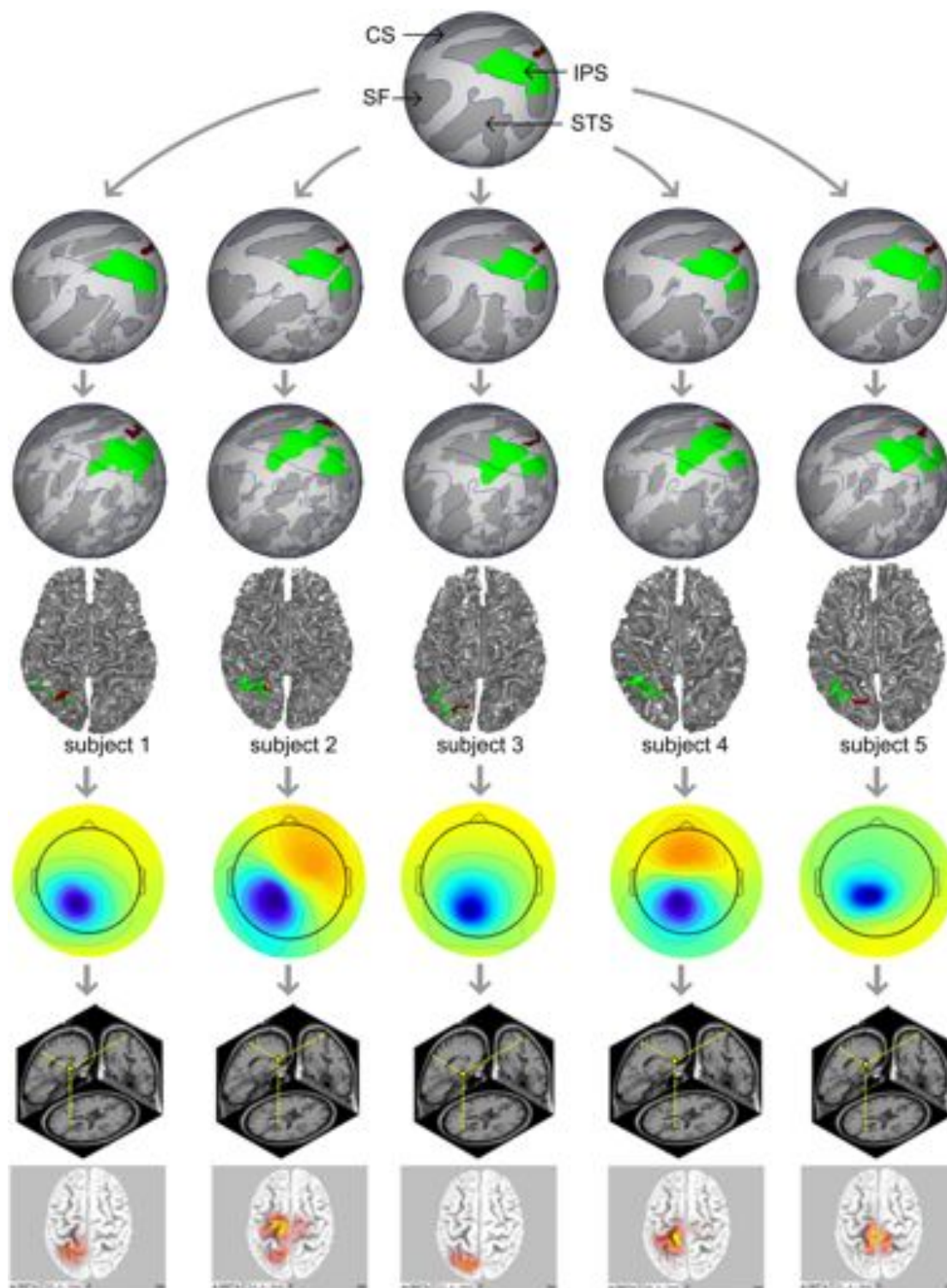


**Figure 1. Differences in cortical locations and scalp maps for functionally equivalent simulated ICs.** (Top) The average fully inflated left cortical hemisphere computed using FreeSurfer (Dale et al., 1999; Fischl et al., 1999) from five individual subjects' inflated and co-registered cortical surfaces after aligning the major cortical sulci (CS, central sulcus; SF, Sylvian fissure; STS, superior temporal sulcus; IPS, intraparietal sulcus), with all sulci shown in

darker grey but IPS in green (labeled using surface-based parcellation proposed by Desikan et al., 2006 and Destrieux et al., 2010). The simulated EEG source consisted of mixture of two Gaussian-tapered patches in the superior parietal gyrus. (2<sup>nd</sup> and 3<sup>rd</sup> rows) The simulated source (darker red) was back-projected to the individual hemisphere after and before alignment, respectively, with an average folding pattern (blue traces). The downward pointing arrows in this figure schematize the simulation steps. (4<sup>th</sup> row) Corresponding source areas on the non-inflated cortical surfaces, showing their spatial disparity though are all located in the superior parietal gyrus near IPS (green). (5<sup>th</sup> row) The computed projections of these five sources to the scalp; note that slight deviations in source orientation produced significantly different scalp projections. (6<sup>th</sup> row) Equivalent current dipoles for these simulated sources fit using EEGLAB dipfit() in a template head model (Delorme and Makeig, 2004). (7<sup>th</sup> row) Results of standardized Low Resolution Brain Electromagnetic Tomography Analysis (sLORETA) (Pascual-Marqui, 2002) applied to each simulated source. Note inter-subject differences in scalp maps, dipole locations, and cortical source density estimates for topologically and therefore possibly functionally equivalent sources.

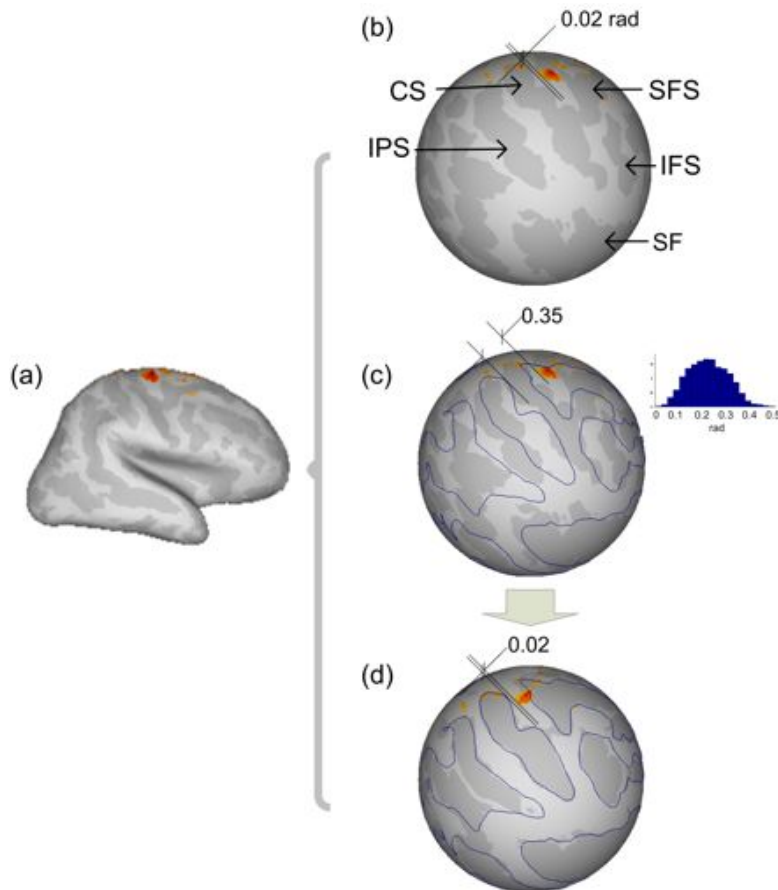


**Figure 2. An IC accounting for precentral mu rhythm (in the rPREC $\mu$  cluster), with and without group cortical alignment, shows differences in active cortical area. (a) The active IC source area in the right hemisphere in the partially inflated cortical model for this subject (Subject 2 in Fig. 1). (b) The subject's fully inflated cortical model (IFS, inferior frontal sulcus; SFS, superior frontal sulcus; other areas as in Fig. 1). The distance in spherical coordinates between the active IC source area and the central sulcus in the native brain is 0.02 rad. (c) Here the blue contours show the average sulcal folding pattern across all subjects. In the average cortical model the distance between the individual active IC source area and the central sulcus is 0.35 rad. The histogram inset demonstrates the distribution of distances between voxels on the individual cortical model to corresponding voxels in the average brain, distances ranging from 0.0 to 0.5 rad. (d) The IC activation area in the subject brain model is warped into the group-aligned cortical model. In this model, the distance of the active source area to the central sulcus remains 0.02 rad. In the clustering procedure, ICs from all subjects are first pooled, the IC pair with the highest pairwise similarity is selected to form a cluster, and all the ICs from these two subjects are excluded from the further selection process. The remaining ICs with the**

*highest pairwise similarity to the two selected ICs are grouped into the cluster; this procedure is continued for other subjects until each of the subjects has one and only one IC selected into the cluster. This clustering procedure is repeated to form more clusters until all components are selected. Test-retest reproducibility analysis (Genovese et al., 1997; Liou et al., 2003) was used to automatically determine the number of clusters.*

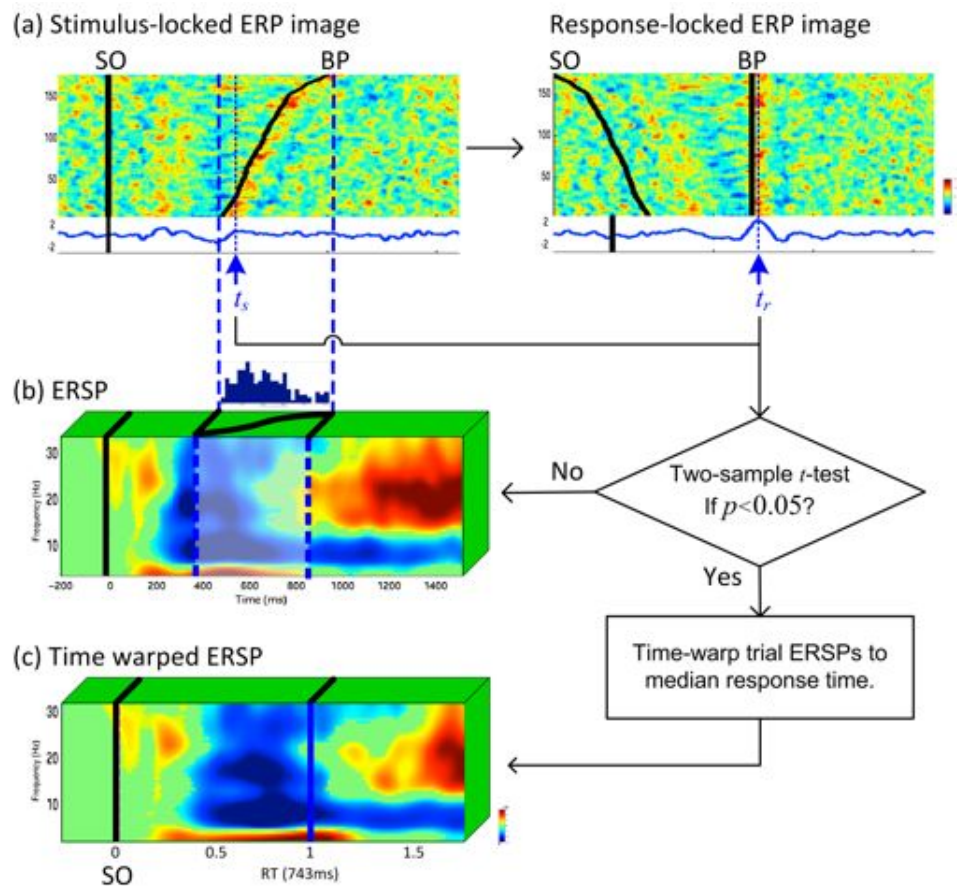


**Figure 3.** An IC in the  $rPREC\mu$  cluster exhibits a mean ERSP difference before and after time warping to both stimulus onsets and button press responses. (a) The reaction-time (RT) sorted ERP-image plots of data epochs showing vertically stacked (and lightly smoothed) epoch activity values from one subject time-locked, respectively, to stimulus onsets (left) and to subject button presses (right) (vertical smoothing, 6 trials). The blue traces below the ERP-image plots give the mean time courses (ERPs). Two blue dashed vertical lines show the RT range; the subplot below (a), the RT histogram. The dotted dark blue vertical lines at  $t_s$  and  $t_r$  in (a) denote the peak latencies of the respective ERPs in the RT range. (b) (green box) A cuboid whose depth represents the multiple single-trial event-related spectral perturbation images time-locked to stimulus onsets. The front face shows the trial-average ERSP. Green portions of the ERSP image are non-significantly different from 0 ( $p < 0.01$ ) by surrogate data testing [Makeig et al., 1993; Jung et al. 2001]. A two-sample t-test was performed to determine whether single-trial activity values at the observed ERP

peak at  $t_s$  (between blue dashed vertical lines) in epochs time-locked to stimulus onset were significantly smaller than in epochs time-locked to the motor response (right) at  $t_r$ . Single-trial ERSPs of those ICs were linearly time-warped prior to IC clustering. (c) The latency-aligned ERSP allows visualization of spectral changes aligned either to stimulus onset (SO) or to the motor response (RT). X-axis units are in multiples of the median reaction time (743 ms).

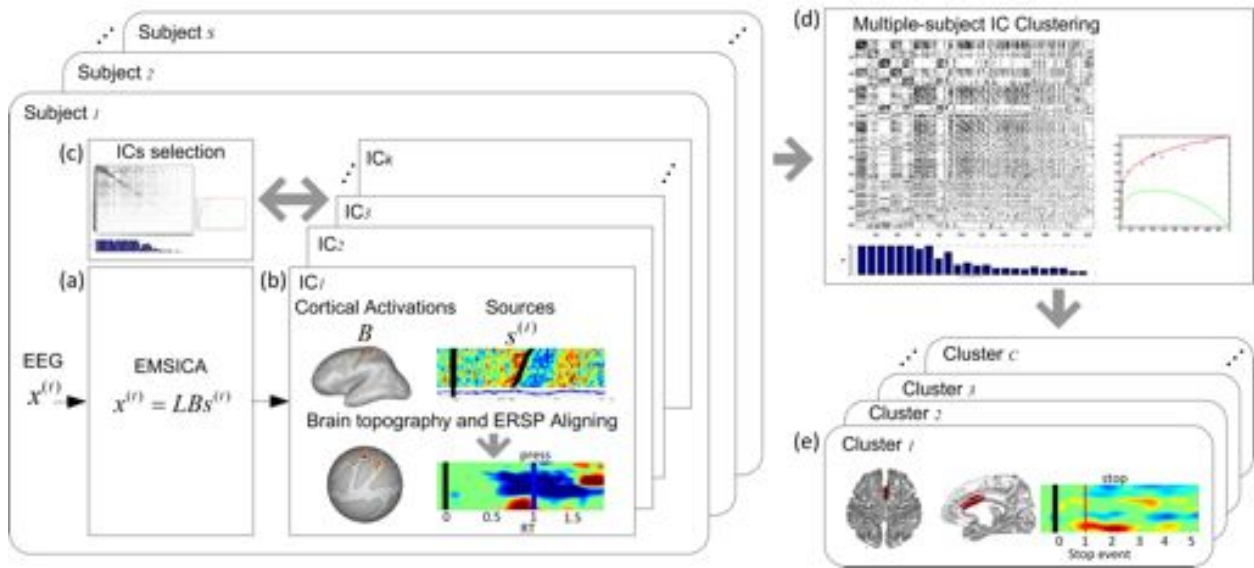


**Figure 4. Multi-subject spatiotemporal cortex- and ERSP latency-aligned IC clustering.** (a) The EMSICA decomposition, which directly and simultaneously estimates spatiotemporally independent cortical source distributions and corresponding cortical field activity time courses for each subject. (b) The decomposed independent components (ICs) are then mapped onto the group-average cortical hemisphere model and time-warped so as to be aligned both to stimulus onsets and to subject button press events. (c) Enhanced RAICAR clustering algorithm (Yang et al., 2008) for analysis of component reproducibility within subjects. Upper row left: between-run correlation matrix rearranged as in the original RAICAR algorithm. Right: ROC (red) and Kappa (green) traces. Bottom: bar chart of the reproducibility index. (d) As in (c) but for component clustering across subjects using reproducibility analysis (lower left) to find the best number of clusters. Upper left: between-subject correlation matrix. (e) Resulting reproducible component clusters (reproducibility index > 75%); spatial extents and averaged brain activation maps. Only cluster components with at least one spatiotemporal correlation coefficient (SCC) higher than the optimized threshold are included in the cluster average.

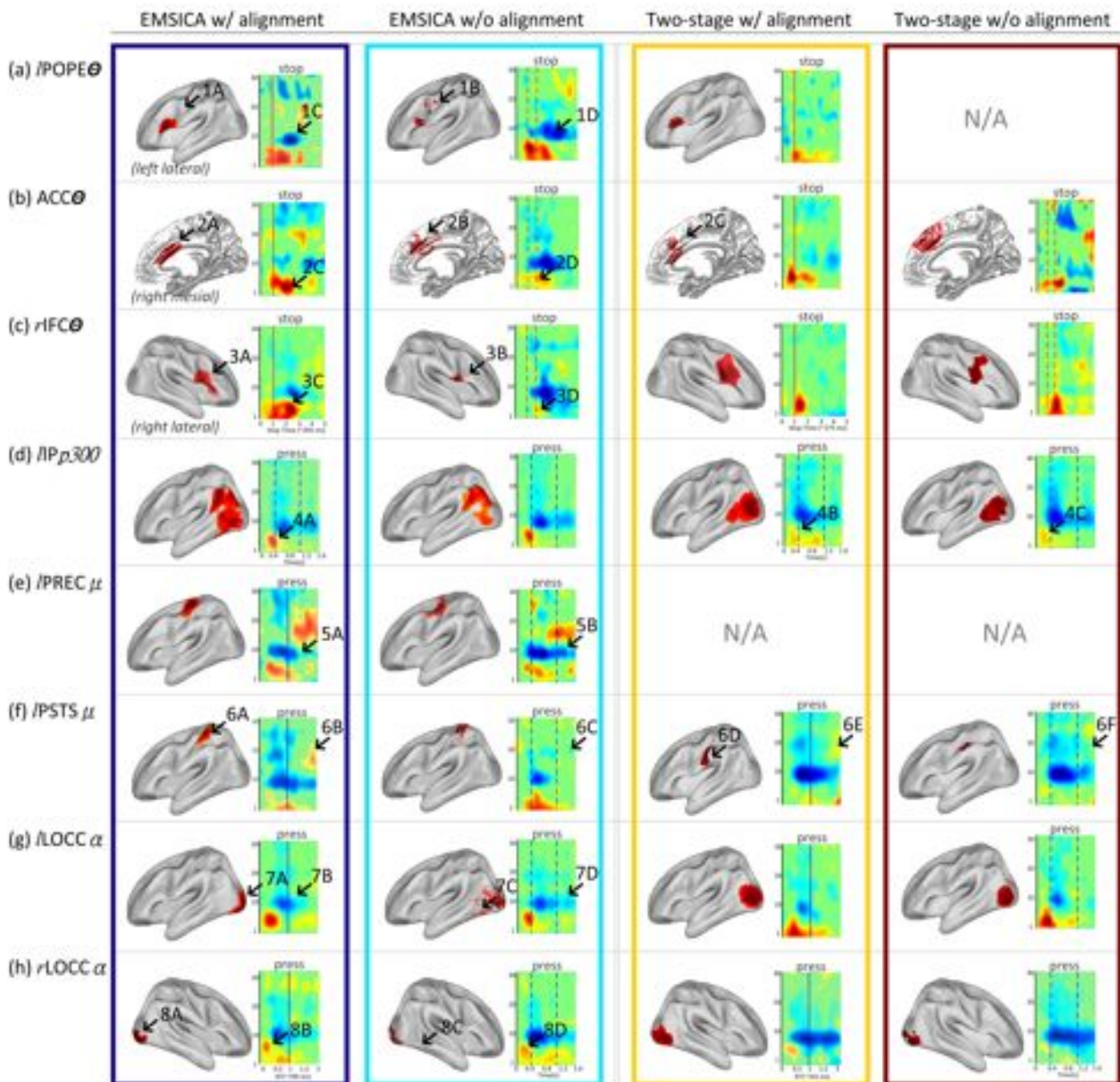


**Figure 5. Eight spatiotemporal component clusters of interest.** Left to right columns show component cluster spatial activity maps and the ERSP images from target stimulus onset (0 ms) for (1) cortex- and latency-aligned EMSICA, (2) non-aligned EMSICA, (3) temporal ICA with alignment, and (4) temporal ICA without alignment on the semi-inflated mean cortical surface ( $\text{IPOPE}\theta$ , left pars opercularis theta;  $\text{ACC}\theta$ , anterior cingulate cortex theta;  $\text{rIFC}\theta$ , right inferior frontal cortex theta;  $\text{IPp300}$ , left inferior parietal P300;  $\text{IPREC}\mu$ , left precentral mu;  $\text{IPSTS}\mu$ , left postcentral mu;  $\text{lLOCC}\alpha$ , left lateral occipital alpha;  $\text{rLOCC}\alpha$ , right lateral occipital alpha).

*l/rLOCC $\alpha$ , left/right lateral occipital alpha. N/A, comparable cluster not available). Regions of interest indicated by arrows are discussed in the text. In these ERSP images, blue dashed vertical pairs of lines show the button-press range (subject response time after 'deer' or 'tank' stimulus onset, ranging from 396 to 1164 ms); red dashed vertical pairs of lines, the stop signal onset time range (latency after 'deer' or 'tank' stimulus onset, ranging from 250 to 538 ms). For component clusters (a-c) (IPOPE $\theta$ , ACC $\theta$ , and rIFC $\theta$ ) and (e-h) (IPREC $\mu$ , IPSTS $\mu$ , and l/rLOCC $\alpha$ ), the single-trial ERSP images were time-warped to a common baseline before averaging across trials and subjects. Blue solid vertical lines mark the latency-aligned button-press (mean subject-median response time after 'deer' or 'tank' stimulus onset, 709 ms); red solid vertical lines mark the stimulus-aligned stop signal onset (mean latency after 'deer' or 'tank' stimulus onset, 295 ms).*

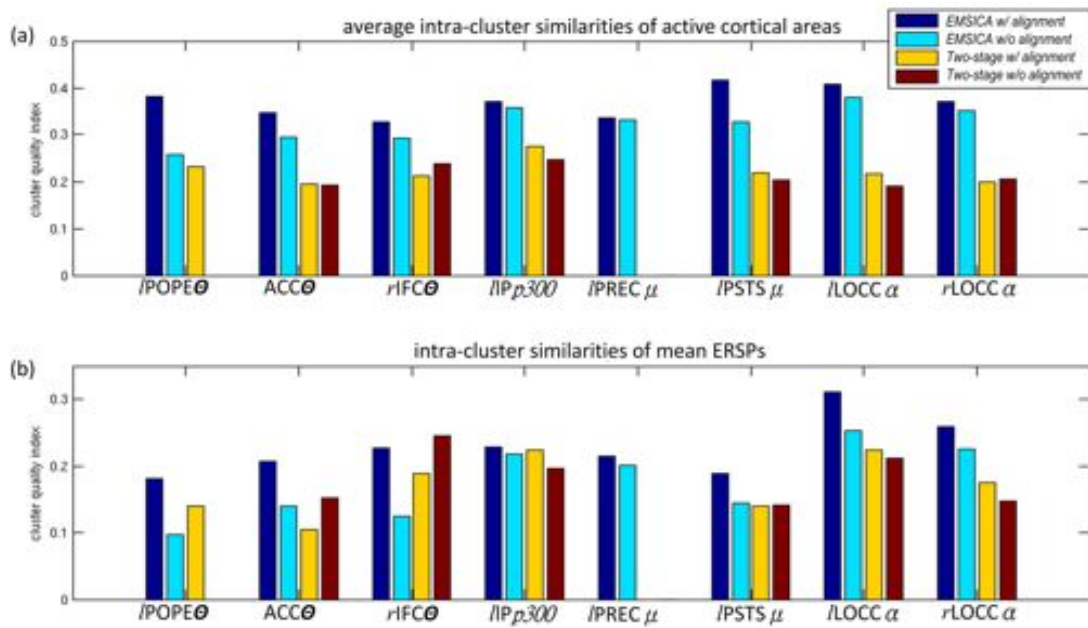


**Figure 6. Compactness of clusters summarizing similarities for all component pairs in each of the eight clusters.** The clusters names are given below the bars. (a) Cluster quality indices assessed by the average intra-cluster similarities of active cortical areas. (b) Cluster quality indices assessed by intra-cluster similarities of mean ERSPs time-locked to stimulus onsets.